Isolation of an energetic monocycle optical pulse in the ultraviolet range

Yuichiro Kida

Phys. Rev. A **96**, 063840 — Published 29 December 2017

DOI: 10.1103/PhysRevA.96.063840

Isolation of an Energetic Monocycle Optical Pulse in the Ultraviolet

Yuichiro Kida[1,2*]

[1] JST PREST, 4-1-8 Honcho, Kawaguchi, Saitama, 332-0012, Japan
[2] RIKEN SPring-8 Center, Koto 1-1-1, Sayo, Hyogo, 679-5148, Japan
E-mail: kida@spring8.or.jp

*To whom correspondence should be addressed.

Abstract

An approach is proposed and numerically investigated to isolate an energetic monocycle pulse in the ultraviolet. The ultraviolet radiation is generated in an attosecond radiation window formed from multicolored, multicycle pulses with mutual phase coherence. Using multiple multicycle pulses with energy scalabilities, the scheme is expected to lead to orders of magnitude higher pulse energy of the monocycle optical radiation than those of the sub-10-fs ultraviolet pulses that have been generated so far. The carrier envelope phase of the monocycle ultraviolet pulse is tailored through the phases of the incident laser radiations.

PACS: 42.65.Re; 42.65.Jx; 42.65.Ky; 42.65.Sf

Ultrashort optical pulses are nowadays available in various wavelength ranges from the x-ray to the infrared. In the ultraviolet (UV) spectral range, several schemes generate ultrashort pulses [1-9], some of which have been applied to probe ultrafast dynamics in molecules [10-14] and ions [15]. The pulse energies of the ultrashort UV pulses reported so far reach one microjoule, while the shortest UV pulse ever generated has a duration shorter than 3 fs [9]. Third-harmonic generation (THG) in a gas medium [1] is employed there, which is initiated by a sub-4-fs pulse, and the available pulse energy is determined by the onset of the photo-ionization [9] as well as the available pulse energy for the sub-4-fs driver. Generation of monocycle pulses in the UV is yet to be demonstrated.

Further shortening the UV pulses towards the single field-oscillation period would allow the excitation of electron wavepackets [16] in the spectral ranges of vacuum-UV and deep-UV for biologically relevant molecules. Higher pulse energy may also be demanded for highly nonlinear interactions such as the ionization [17-19] as well as those generate shorter-wavelength radiations. The UV pulse may also seed the proposed scheme of the monocycle harmonic generation in free-electron lasers that is expected to generate isolated monocycle pulses there [20].

In this Letter, we propose an approach to generate isolated UV pulses with monocycle pulse durations with scalable pulse energies. In contrast to precedent schemes that are based on the light-matter interactions in femtosecond time scales [9], the idea presented here creates an attosecond radiation window within which UV radiations are confined to form an isolated light transient with the comparable duration. This transient window is formed after combining a train of monocycle pulses synthesized from multicycle, multicolored optical pulses and a longer pulse with scalable pulse energies. The scheme mainly relies on four-wave mixing (FWM) for highly efficient frequency up-conversion. Numerical investigations presented in this letter show practical examples of the scheme and the characteristics of the monocycle UV pulses to be generated there.

In the proposed scheme, a train of monocycle pulses and a relatively long laser pulse, the latter of which is hereafter called a gate pulse, are first prepared in the visible to near-infrared (NIR) spectral ranges [(A) in Fig. 1(a)]. The train of monocycle pulses, for instance, can be generated via FWM in a gas medium followed by the Fourier synthesis of the generated multicolor laser lines [21-24]. The gate pulse assumed here is longer than the monocycle pulse but short enough compared to the separation between two adjacent monocycle pulses in the train. As illustrated in Fig. 1 (a), when degenerate FWM is induced by the pulses in a transparent medium, the gate pulse nonlinearly slices the temporal fraction where it coincides with one of the monocycle pulses in the train for frequency up-conversion into the UV: which is hereafter referred to as nonlinear optical-pulse slicing (NOPS). Since the FWM is a third-order nonlinear interaction, the UV radiation is confined within a temporal window with a duration much narrower than any of the gate pulse and the monocycle pulses in the train. To be specific, as illustrated in Fig. 1(b), the radiation is confined within the cube (solid line) of the intensity of the incident radiation (dotted line) synthesized by the pulse train and the gate pulse, which has an attosecond duration determined by the wavelengths of the constituent spectral components.

The numerical simulation in this research relies on the forward Maxwell equation that directly treats the evolution of electric field [25-27]. For propagation in a gas-filled hollow fiber, the equation for the longitudinal field component $\widetilde{E}(z,\omega)$ may be written with the moving frame at a velocity v_g [25]:

$$\frac{\partial \widetilde{E}(z,\omega)}{\partial z} = \{i[\beta(\omega)-\frac{\omega}{v_g}]-\alpha(\omega)\}\widetilde{E}(z,\omega)+\frac{i}{2\beta(\omega)}\frac{\omega^2}{\varepsilon_0 c^2}\frac{\int A(x,y)^4 F\{P^{NL}(z,t)\}dxdy}{\int A(x,y)^2 dxdy}$$
$$-\frac{n(\omega_0)\omega}{2\beta(\omega)c}\frac{1}{\int A(x,y)^2 dxdy}\int A(x,y)^2[U_i F\{W(\rho_{nt}-\rho)E(z,t)/I\}-[1+i\omega\tau_c(x,y)]\sigma(x,y,\omega)F\{\rho E(z,t)\}]dxdy \quad , \qquad (1)$$

with the time-evolution of the electron density:

$$\frac{\partial \rho}{\partial t} = W(I)(\rho_{nt} - \rho) + \frac{\sigma}{U_i}\rho I \cdot \tag{2}$$

$A(x, y)$ is the transverse field component, the nonlinear polarization $P^{NL}(z,t) = \varepsilon_0 \chi^{(3)} E^3(t)$ is of the third-order nonlinearity [28,29], and the integrals account for the nonlinearity reduction [25,28]. The frequency-dependent propagation constant or eigen value $\beta(\omega)$ has contributions from the material (gas) and the waveguide (hollow fiber) [30]. The extinction coefficient $\alpha(\omega)$ accounts for the propagation loss for the guided mode, and $n(\omega_0)$ is the refractive index of the medium at the carrier frequency of the electric field.

The wave equation is numerically solved with the split-step Fourier method and the fourth-order Runge-Kutta method for the nonlinear step [25,31] assuming the guided mode of EH_{11} for $A(x, y)$ [30]. Argon is assumed throughout in this letter as the gas medium filled in the hollow core with a diameter of 320 μm, and the wavelength-dependent refractive index of it is calculated with the dispersion parameters in [32]. The nonlinear refractive index of argon is $1 \times 10^{-19}\ p$ cm^2/W where p is the ratio of the argon pressure to one atmosphere [33]. The pressure of the argon gas is assumed to be 0.019 bar. W is the ionization rate calculated with the Keldysh-PPT formalism [26,27,34] using the carrier frequency and the time-dependent field amplitude of the electric field [26,33], U_i is the ionization potential, $\rho = \rho(x, y, t)$ and ρ_{nt} are the electron density and the initial density of neutral species being the ideal gas, respectively. $F\{\}$ shows Fourier transform, c is the speed of light in vacuum, ε_0 is the vacuum permittivity, and $I = I(x, y, z, t)$ is the intensity of the laser pulse. The electron-neutral collision time τ_c for the inverse Bremsstrahlung is calculated with the hard-sphere model [35] and the van der Waals radius given in [36], while the cross section σ is calculated by the Drude model in the numerical simulation [27,37].

The ionization effects have nontrivial contributions in the intensity range assumed in this research, and hence are always involved in the numerical simulations. In fact, the above model leads to a pulse energy of 0.3 μJ that is close to the experimental value of 0.5 μJ for the UV radiation generated after the THG in argon driven by a 6-fs pulse with an intensity of 4×10^{14} W/cm^2 [8]. The simulation overestimates the energy by an order of magnitude when the ionization-related terms are dropped from the equation.

To simulate the NOPS scheme, three multicycle pulses with pulse durations of 50 fs and central wavelengths of 1200, 800, and 600 nm are assumed to be temporally overlapped with each other without relative time delays to form a train of monocycle pulses with a duration of 2.7 fs and a repetition period of 8 fs. The pulse energy assumed in each is 75 μJ for 1200 and 600 nm, and 150 μJ for 800 nm, respectively. Such three-color radiations may be prepared by four-wave mixing in gases with a mutual phase coherence [38,39]. A shorter multicycle pulse with a duration of 8 fs, a central wavelength of 400 nm, and a pulse energy of 150 μJ is assumed to be the gate pulse. The pulse shapes of these spectral components are of the sech function, and the carrier-envelope phases (CEPs) of all the incident radiations are assumed to be zero to form carrier waves with cosine functions. The pulse train and the gate pulse are assumed to be simultaneously coupled with no relative time delay with respect to each other into the argon-filled hollow fiber with a length of 380 mm to simulate the profile of the UV laser radiation generated in the hollow fiber under the frame of reference propagating at the group velocity at 800 nm.

As shown in Fig. 2(a), the simulated spectrum of the output laser radiation from the hollow fiber forms a continuum spanning from the NIR to the vacuum-UV. It consists of the input radiations [(i), (ii)] and the UV radiation generated in the hollow fiber [(iii)]. The temporal intensity profile of the UV continuum in the wavelength range of 133−320 nm is of an isolated pulse with a duration (full width at half maximum, FWHM) of 1.4 fs or a 1.7-cycle pulse with a carrier wavelength of 250 nm. The temporal profile was calculated after applying a hard-edge spectral filter to the output radiation, extracting the UV continuum. The pulse is slightly longer than the transform-limited duration of 1.2 fs calculated from the spectrum. The pulse energy of the UV pulse is 7.5 μJ or 5% of that of the incident gate pulse. If the relative phase

between the gate pulse and the pulse train remains unchanged, the temporal intensity profile of the UV pulse does not vary appreciably. This is illustrated in Fig. 2(b) in which the temporal intensity profiles of the UV radiations are calculated for 9 different CEPs of the input radiations of ϕ_t = 0, π/8, π/4, π/2, 3π/4, π, 5π/4, 3π/2, and 7π/4 with a fixed relative phase, i.e., $\phi_t = \phi_g$ with the CEP of the pulse train of ϕ_t and that of the gate pulse of ϕ_g, respectively. This stability against the CEP variation relates to the fact that the intensity of the UV radiation generated via the FWM is proportional to the square of the nonlinear polarization. In other words, the intensity is proportional to the cube of the intensity of the incident synthesized field. The temporal intensity profile of the incident laser radiation synthesized from the pulse train and the gate pulse does not vary with a change in the CEPs provided that the relative phase remains unchanged. The temporal intensity profile of the UV radiation is therefore not sensitive to the CEPs but to the relative phase. This scenario may be valid if the contribution of THG is negligibly small compared to that of the FWM. In general, much higher efficiencies are experimentally reported for FWM [2,38,40,41] than that for THG [1,4,8,42]. Numerical simulations on THG induced by a NIR pulse with the same intensity as that for the incident synthesized pulse for the NOPS have implied that the contribution from THG is at least an order of magnitude smaller than the FWM (data not shown).

There is, however, slight variation in the temporal intensity profile with a change in the CEP [slight deviation among the solid lines in Fig. 2(b)]. This may relate to the interference between the FWM and the weak THG. Given the CEP of the incident synthesized radiation of ϕ_{in}, the FWM or self-phase modulation (SPM) induced by the synthesized intense radiation, shares this ϕ_{in}. On the one hand, the THG generates radiation with a phase of $3\phi_{in} + \pi/2$. The relative phase between the two radiations generated from the FWM and THG varies as a function of $2\phi_{in}$, which, through the interference, should result in the slight variation in the temporal intensity profile shown in the figure. For $\phi_{in} = 0$ and $\phi_{in} = \pi$, the relative phases become identical and expected to give the identical intensity profile of the synthesized field. Both the temporal intensity profiles and spectra of the UV radiations simulated for these two specific cases have indeed completely coincided.

The UV radiation is generated as if no monocycle pulses existed in the pulse train except the one temporally overlapped with the gate pulse. This is visualized in Fig. 2(b) in which the temporal intensity profile of the UV radiation is calculated for the same interaction as above but after the replacement of the pulse train by a purely isolated monocycle pulse with the same pulse duration and intensity. The pulse duration of the UV radiation is 1.6 fs which is close to the duration of the UV radiation in the NOPS. Both the UV radiations from the two schemes have similar structures except the weak pedestal component that is present only for the NOPS scheme.

The pulse duration of the UV radiation depends on the propagation length in the hollow fiber as well as the width of the radiation window discussed above. This is because the group-velocity dispersion (GVD) tends to broaden the UV pulse duration. During the propagation in the fiber, the incident synthesized pulse changes its shape from a single-peak structure (a) to dual peaks (d) during the propagation as shown in Figs. 3(a-d). The variation originates from the change in the relative phase between the pulse train and the gate pulse due to the GVD. To be specific, the pulse shape at the propagation distance z of 127 mm [Fig. 3 (b)] is similar to that of the incident radiation with the relative phase of π/2 shown in Fig. 3(f), while the profile in Fig. 3(d) is close to that with the relative phase of π in Fig. 3(g). Owing to the change in the shape during the propagation, the UV pulse is delayed with respect to the peak of the synthesized field intensity within which the UV radiation is initially generated. The delay leads to the pulse duration of the UV pulse at the exit of the fiber (1.4 fs) that is longer than the radiation window formed by the incident synthesized radiation (0.75 fs). The complete separation of the UV radiation peak from the input radiation peak at the exit of the fiber [Fig. 3(d)] saturates the growth of the peak intensity of the UV radiation. The temporal intensity profile of the UV pulse is also sensitive to that of the incident synthesized pulse. For instance, both the input [Fig. 3(g)] and output UV [Fig. 3(j)] radiations have two peaks when the CEPs of the pulse train and the gate pulse, respectively, are $\phi_t = 0$ and $\phi_g = \pi$.

Higher pulse energies of the input pulses lead to a higher efficiency in the energy conversion from the gate pulse

into the UV radiation. The numerical simulation for the NOPS has been repeated with 5-times and 10-times higher input intensities [Fig. 4(a)]. The temporal intensity profiles of the UV radiations in the two cases also have isolated pulse structures with similar durations of 1.8 fs and 1.5 fs after propagation lengths of 70 mm and 51 mm, respectively. Since the NOPS relies on the third-order nonlinearity, the conversion efficiency is sensitive to the intensity. The energy conversion efficiencies from the gate pulse to the UV radiation in the former and the latter, respectively, are 10% and 20%. The latter corresponds to the pulse energy of the UV radiation of 290 μJ, and the peak intensity of the UV radiation saturates after the complete depletion of the portion of the gate pulse which coincides with the incident monocycle pulse. The main peak in the pulse train, which is responsible for the generation of the UV radiation, is also depleted there. Such depletion is not observed in numerical simulations with dropped source terms related to photo-ionization, resulting in the propagation of the UV radiation without the saturation. The pulse duration of the UV radiation is also affected by the photo-ionization: which is a different regime from the above NOPS with the lower intensity of the incident radiations. Since the depletion terminates the energy flow into the UV radiation, the UV pulse should propagate over a certain distance after the saturation without notable variation in the temporal profile. The numerical simulation indeed showed such a stable propagation. Since the confocal parameter of the incident laser beam at 1200 nm is calculated to be 56 mm, free-space focusing geometry may be applied rather than the use of a hollow fiber in this highly nonlinear regime.

Stable propagation of an isolated sub-2-fs DUV pulse was also theoretically investigated in a previous research for the FWM in the filamentation regime [43]. Similar to the above NOPS situations, incident laser pulses with a millijoule-level energy is assumed there, but to induce the self-channeling enabling the nonlinear propagation over a long distance. Even with the simpler scheme proposed for the self-compression with only the two-color, multi-cycle incident radiations, a sub-2-fs DUV pulse is predicted to emerge with a pulse energy of 15 μJ after a long propagation distance in excess of 1 m. The short pulse duration is retained in the subsequent propagation over 300 mm without a significant reduction in the intensity [43]. In the NOPS scheme, on the other hand, an isolated sub-2-fs DUV pulse emerges at the beginning of the propagation, and the short pulse duration is retained in the subsequent propagation during which the peak intensity increases. A combination of the NOPS and the filamentation regime might lead to propagation of sub-2-fs DUV pulses over a longer propagation distance than those in the present research and the filamentation regime: which is beyond the scope of the present research (and the future works that follow).

For a locked relative phase between the pulse train and gate pulse, the incident spectral components at 1200, 800, 600, and 400 nm may be, for instance, generated from a CEP-stable Ti:sapphire chirped-pulse amplifier (CPA) followed by frequency conversions with white-light-seeded optical parametric amplifiers (OPA) and second-harmonic generation. When the CEP of the Ti:sapphire CPA is not stable, an alternative scheme may be applied: generation of all the necessary spectral components through a white-light seeded OPA or FWM. One of the practical examples uses three laser radiations at 1200 nm (50 fs), 800 nm (50 fs), and 600 nm (8 fs, gate pulse). There, the two radiations at 1200 nm and 600 nm are seeded with a white-light generated by focusing the Ti:sapphire laser radiation (800 nm) into a transparent medium, followed by amplification via OPA pumped at 800 nm and 400 nm. The pulse energies assumed here are 300 μJ for each spectral component at 1200 nm and 800 nm, while 200 μJ at 600 nm. The electric field of the monocycle UV radiation to be generated after the propagation in the argon-filled hollow fiber at a propagation distance of 575 mm is simulated for the CEPs of $\phi_t = \phi_g = 0$ in Fig. 4 (b). The temporal profile was calculated after applying a hard-edge spectral filtering that extracts the spectral components in a range of 133-500 nm. Owing to the reduction in the number of the incident spectral components, the width of the radiation window is stretched to 1.2 fs. The generated UV radiation has a carrier wavelength of 360 nm, and a pulse duration of 1.1 fs or a monocycle pulse duration. The pulse energy is 37 μJ, majority of which is coming from long-wavelength components out of the full radiation range of 133–500 nm.

The point in the NOPS is to form a temporal window with a single peaked structure with an extremely short width

while preventing the formation of intense satellite-pulse structures. If this requirement is met, any sets of wavelengths may be acceptable as the input radiations in NOPS. For instance, the radiation window may be formed from a gate pulse at 800 nm and two multicycle pulses at 600 nm and 1200 nm. Such a generalized NOPS may be discussed in terms of SPM induced by the incident synthesized pulse: the FWM becomes SPM when all the three input electric fields in the FWM are identical. Within the temporal window given by the synthesized field, SPM generates a new frequency component whose intensity is proportional to the cube of it. The NOPS therefore may be regarded as SPM induced by a laser pulse as short as about 1 fs. This corresponds to the situation where the generation of UV continuum by a 12-fs excitation pulse in Ref. [5] is realized with an order of magnitude shorter input and output UV pulses.

The monocycle UV pulse generated in the NOPS may be directly used without filtering out the input spectral components, for instance, for seeding free-electron lasers. Seeding the high-gain harmonic generation scheme [44,45] may give wavelength tunability or multicolor radiations with mutual phase coherence. The UV pulse with the tailored CEP may lead to an access to the CEP of the monocycle pulses from the free-electron lasers based on the monocycle harmonic generation [20]. To separate the UV radiation from the incident radiations, the 4-f zero-dispersion geometry with diffraction gratings and curved mirrors may be applied with a broad bandwidth and a moderate throughput reached by the available gratings in the UV range.

In conclusion, we have proposed a concept of nonlinear optical pulse slicing that leads to generation of an isolated monocycle pulse in the UV. It requires only multicycle laser pulses and has a potential of generation of monocycle pulses with energies orders of magnitude higher than currently available ultrashort UV sources. Such an energetic monocycle source should pave the way to various sciences and technologies involving nonlinear light-matter interactions and seeded FELs.

Acknowledgments

This work was supported by JST PREST Grant Number JPMJPR16P5, Japan.

References

[1] S. Backus, J. Peatross, Z. Zeek, A. Rundquist, G. Taft, M. M. Murnane, and H. C. Kapteyn, Opt. Lett. **21**, 665 (1996).

[2] C. G. Durfee, S. Backus, H. C. Kapteyn, and M. M. Murnane, Opt. Lett. **24**, 697 (1999).

[3] P. Baum, S. Lochbrunner, and E. Riedle, Opt. Lett. **29**, 1686 (2004).

[4] T. Fuji, T. Horio, and T. Suzuki, Opt. Lett. **32**, 2481 (2007).

[5] S. A. Trushin, K. Kosma, W. Fuß, and W. E. Schmid, Opt. Lett. **32**, 2432 (2007).

[6] Y. Kida, J. Liu, T. Teramoto, and T. Kobayashi, Opt. Lett. **35**, 1807 (2010).

[7] R. B. Varillas et al., Opt. Lett. **39**, 3849 (2014).

[8] U. Graf, M. Fiess, M. Schultze, R. Kienberger, F. Krausz, and E. Goulielmakis, Opt Express **16**, 18956 (2008).

[9] F. Reiter et al., Opt. Lett. **35**, 2248 (2010).

[10] K. Kosma, S. A. Trushin, W. Fuss, and W. E. Schmid, J. Phys. Chem. A **112**, 7514 (2008).

[11] K. Kosma, S. A. Trushin, W. Fuss, and W. E. Schmid, Phys. Chem. Chem. Phys. **11**, 172 (2009).

[12] T. Fuji, Y.-I. Suzuki, T. Horio, T. Suzuki, R. Mitrić, U. Werner, and V. Bonac□ić-Koutecký, J. Chem. Phys. **133**, 234303 (2010).

[13] T. Kobayashi and Y. Kida, Phys. Chem. Chem. Phys. **14**, 6200 (2012).

[14] B. Xue, A. Yabushita, and T. Kobayashi, Phys. Chem. Chem. Phys **18**, 17044 (2016).

[15] S. Kahra et al., Nat. Phys. **8**, 238 (2012).

[16] T. Okino, Y. Furukawa, Y. Nabekawa, S. Miyabe, A. Amani Eilanlou, E. J. Takahashi, K. Yamanouchi, and K. Midorikawa, Sci. Adv. **1**, e1500356 (2015).

[17] T. Shimizu, Y. Watanabe-Ezoe, S. Yamaguchi, H. Tsukatani, T. Imasaka, S. Zaitsu, T. Uchimura, and T. Imasaka, Anal. Chem. **82**, 3441 (2010).

[18] A. Hamachi, T. Okuno, T. Imasaka, Y. Kida, and T. Imasaka, Anal. Chem. **87**, 3027 (2015).

[19] P. Sandor, V. Tagliamonti, A. Zhao, T. Rozgonyi, M. Ruckenbauer, P. Marquetand, and T. Weinacht, Phys. Rev. Lett. **116**, 063002 (2016).

[20] T. Tanaka, Phys. Rev. Lett. **114**, 044801 (2015).

[21] M. Y. Shverdin, D. R. Walker, D. D. Yavuz, G. Y. Yin, and S. E. Harris, Phys. Rev. Lett. **94**, 033904 (2005).

[22] W. J. Chen, Z. M. Hsieh, S. W. Huang, H. Y. Su, C. J. Lai, T. T. Tang, C. H. Lin, C. K. Lee, R. P. Pan, C. L. Pan, and A. H. Kung, Phys. Rev. Lett. **100**, 163906 (2008).

[23] K. Yoshii, J. K. Anthony, and M. Katsuragawa, Light-Sci. Appl. **2**, e58 (2013).

[24] Y. Kida and T. Imasaka, Opt. Express **23**, 12373 (2015).

[25] A. V. Husakou and J. Herrmann, Phys. Rev. Lett. **87**, 203901 (2001).

[26] L. Bergé, S. Skupin, R. Nuter, J. Kasparian, and J. P. Wolf, Rep. Prog. Phys. **70**, 1633 (2007).

[27] A. Couairon and A. Mysyrowicz, Phys. Rep. **441**, 47 (2007).

[28] I. V. Babushkin, F. Noack, and J. Herrmann, Opt. Lett. **33**, 938 (2008).

[29] A. A. Voronin and A. M. Zheltikov, Phys. Rev. A **90**, 043807 (2014).

[30] E. A. J. Marcatili and R. A. Schmeltzer, Bell Syst. Tech. J. **43**, 1783 (1964).

[31] G. Agrawal, Nonlinear Fiber Optics (Academic Press, 2006), 4 edn.

[32] A. Dalgarno and A. E. Kingston, Proc. R. Soc. A. **259**, 424 (1960).

[33] S. Skupin, G. Stibenz, L. Berge, F. Lederer, T. Sokollik, M. Schnurer, N. Zhavoronkov, and G. Steinmeyer, Phys. Rev. E. **74**, 056604 (2006).

[34] A. M. Perelomov, V. S. Popov, and M. V. Terentev, Sov. Phys. JETP **23**, 924 (1966).

[35] P. Sprangle, E. Esarey, and J. Krall, Phy. Rev. E **54**, 4211 (1996).

[36] A. Bondi, J. Phys. Chem. **68**, 441 (1964).

[37] E. Yablonovitch and N. Bloembergen, Phys. Rev. Lett. **29**, 907 (1972).

[38] F. Theberge, N. Akozbek, W. Liu, A. Becker, and S. L. Chin, Phys Rev Lett **97**, 023904 (2006).

[39] K. Motoyoshi, Y. Kida, and T. Imasaka, Appl. Sci. **4**, 318 (2014).

[40] C. G. Durfee, L. Misoguti, S. Backus, H. C. Kapteyn, and M. M. Murnane, J. Opt. Soc. Am. B **19**, 822 (2002).

[41] A. E. Jailaubekov and S. E. Bradforth, Appl. Phys. Lett. **87**, 021108 (2005).

[42] C. G. Durfee, S. Backus, M. M. Murnane, and H. C. Kapteyn, Opt. Lett. **22**, 1565 (1997).

[43] L. Bergé and S. Skupin, Opt. Lett. **33**, 750 (2008).

[44] E. Allaria et al., New J. Phys. **14**, 113009 (2012).

[45] E. Allaria et al., J. Synch. Rad. **22**, 485 (2015).

Figures

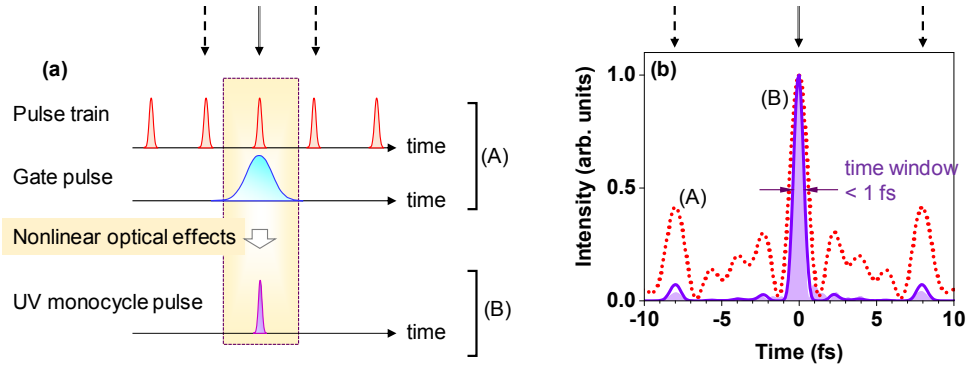

Figure 1

Yuichiro Kida

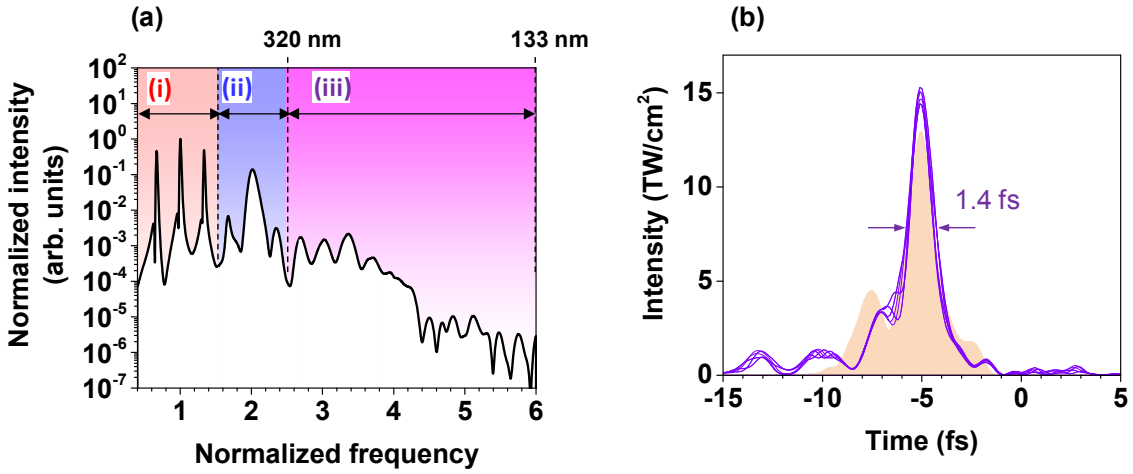

Figure 2

Yuichiro Kida

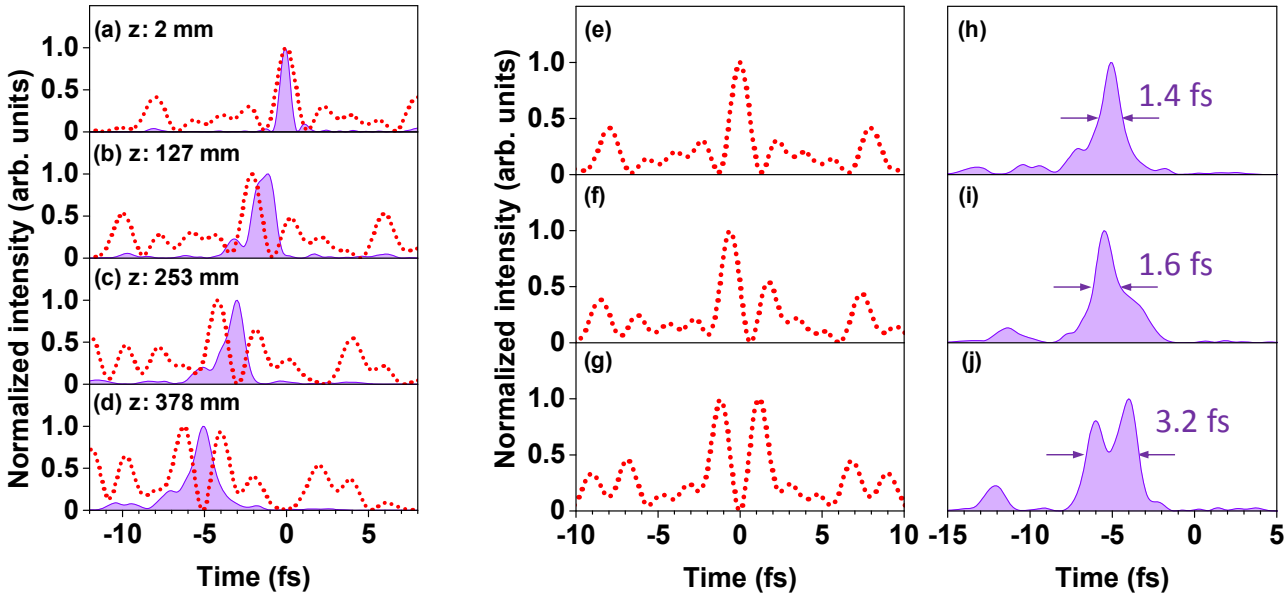

Figure 3

Yuichiro Kida

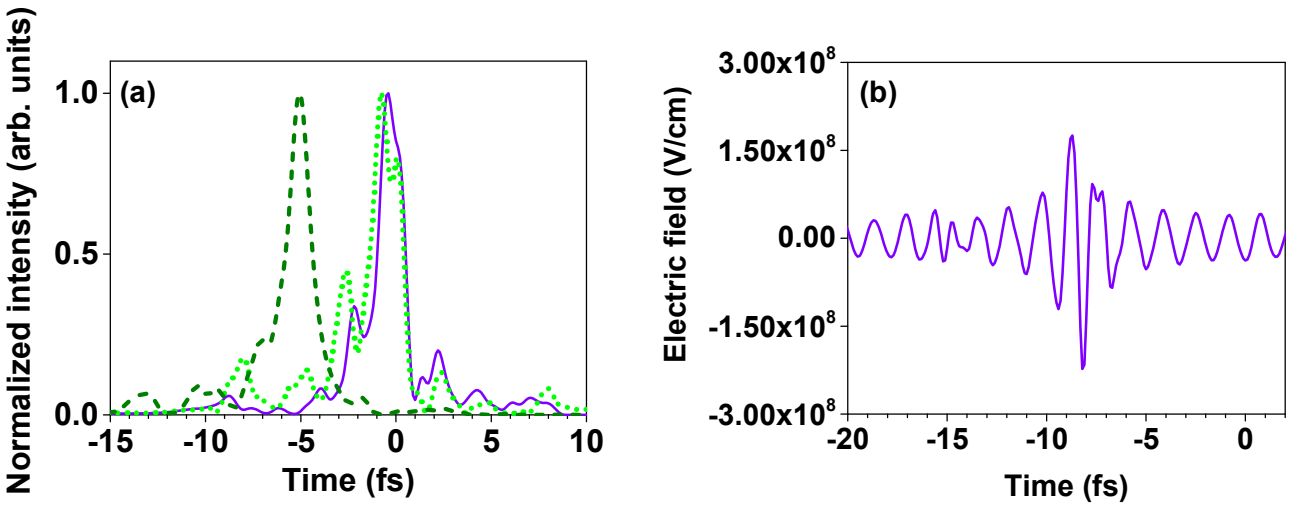

Figure 4

Yuichiro Kida

Figure captions

FIG. 1. (a) Schematic illustration of NOPS scheme. (b) Intensity of the incident synthesized pulse (dotted line, A), the attosecond time window (solid line, B), and the intensity of the UV radiation (solid area), which are the simulation results in Fig. 3(a) for the propagation length of 2 mm. Vertical arrows show the locations of the incident monocycle pulses.

FIG. 2. Simulated (a) spectral and (b) temporal profiles. In (a), the frequency is normalized by that corresponds to a wavelength of 800 nm. The spectral regions (i), (ii), and (iii), respectively, are of the incident pulse train, gate pulse, and the generated UV radiation. In (b), the temporal intensity profiles of the UV radiations simulated for the 9 different phases are shown with solid lines. Solid area is the profile of the UV radiation generated by use of the pure isolated monocycle pulse and the gate pulse.

FIG. 3. (a-d) Simulated temporal intensities of the incident synthesized pulses (dotted line) and the UV radiation at propagation distances of (a) 2, (b) 127, (c) 253, and (d) 378 mm, respectively. Simulated temporal intensities of (e-g) the incident synthesized pulses at the entrance and (h-j) the UV radiations at the exit of the fiber (h-j). The CEPs of the incident radiations are: (e, h) $\phi_t = \phi_g = 0$; (f, i) $\phi_t = \pi/2$, $\phi_g = 0$; (g, j) $\phi_t = 0$, $\phi_g = \pi$.

FIG. 4. (a) Normalized temporal intensity profiles of the UV radiations simulated for the gate-pulse intensities of 0.76 (broken line), 2.3 (dotted line), and 7.6×10^{14} W/cm^2 (solid line), respectively. (b) Simulated electric field of the UV radiation generated in the NOPS with the three incident spectral components.